nature physics

Article

https://doi.org/10.1038/s41567-023-02014-6

Memory and rejuvenation effects in spin glasses are governed by more than one length scale

Received: 12 July 2022

Accepted: 7 March 2023

Published online: 27 April 2023

Check for updates

M. Baity-Jesi[1], E. Calore[2], A. Cruz[3,4], L. A. Fernandez[5], J. M. Gil-Narvion[4], I. Gonzalez-Adalid Pemartin[5], A. Gordillo-Guerrero[6,7], D. Iñiguez[3,4,8], A. Maiorano[9,10], E. Marinari[10,11,12], V. Martin-Mayor[5], J. Moreno-Gordo[3,4,13], A. Muñoz Sudupe[5], D. Navarro[14], I. Paga[15] ✉, G. Parisi[10,11,12], S. Perez-Gaviro[3,4], F. Ricci-Tersenghi[10,11,12], J. J. Ruiz-Lorenzo[7,13], S. F. Schifano[16], B. Seoane[5,17], A. Tarancon[3,4] & D. Yllanes[4,18]

Memory and rejuvenation effects in the magnetic response of off-equilibrium spin glasses have been widely regarded as the doorway into the experimental exploration of ultrametricity and temperature chaos. Unfortunately, despite more than twenty years of theoretical efforts following the experimental discovery of memory and rejuvenation, these effects have, thus far, been impossible to reliably simulate. Yet, three recent developments convinced us to accept this challenge: first, the custom-built Janus II supercomputer makes it possible to carry out simulations in which the very same quantities that can be measured in single crystals of CuMn are computed from the simulation, allowing for a parallel analysis of the simulation and experimental data. Second, Janus II simulations have taught us how numerical and experimental length scales should be compared. Third, we have recently understood how temperature chaos materializes in aging dynamics. All these three aspects have proved crucial for reliably reproducing rejuvenation and memory effects on the computer. Our analysis shows that at least three different length scales play a key role in aging dynamics, whereas essentially all the theoretical analyses of the aging dynamics emphasize the presence and crucial role of a single glassy correlation length.

The remarkable off-equilibrium behaviour of glass formers at low temperatures has been described with terms such as aging[1] or memory and rejuvenation[2–5], which seem more suitable for living beings than for inert chunks of matter. In this context, spin glasses (which are disordered magnetic alloys[6]) enjoy a privileged status. On the experimental side, their magnetic response can be studied with great accuracy using a superconducting quantum interference device. Rejuvenation and memory (as described below) are, furthermore, remarkably strong in spin glasses, probably because of the large correlation length ξ of coherent spin domains. The values of ξ achieved in single-crystal samples[7–10] is much larger than in other glass-forming materials (for instance, the ξ value measured in supercooled glycerol or propylene carbonate[11] is smaller by a factor of ~100). On the other hand, spin-glass theory[12] has proven to be applicable to distant fields that also feature rugged free-energy landscapes, such as combinatorial optimization, machine learning, biology, financial markets or social dynamics.

A full list of affiliations appears at the end of the paper. ✉e-mail: ilaria.paga@gmail.com

It is worth stressing that the main part of spin-glass experimental studies is carried out under off-equilibrium conditions[13]. In the simplest setting, the so-called zero-field-cooling (ZFC) protocol, the system is initially at equilibrium at some very high temperatures. Eventually, the spin glass is abruptly cooled to the working temperature $T < T_g$ and relaxes for a waiting time t_w (T_g is the glass temperature and t_w ranges from minutes to several hours). At time t_w, a magnetic field H is switched on and the growing magnetization $M_{ZFC}(t, t_w)$ is recorded at later times of $t + t_w$. $M_{ZFC}(t, t_w)$ has turned out to have a notable dependence on t_w for as long as researchers have had the patience to wait. The relaxation rate is given by

$$S_{ZFC}(t, t_w; H) = \frac{1}{H}\frac{dM_{ZFC}(t, t_w; H)}{d\log t} \quad (1)$$

peaks at a time $t^{eff}{}_H$ roughly equal to t_w (experimental results shown elsewhere[9,10]). The only relevant timescale that can be identified is the age of the glass, namely, t_w (and hence the term aging). Figure 1 (left) shows our results for this comparatively simple fixed-temperature protocol, which will be named native hereafter. The native setup is used as a standard for comparison.

Quest for rejuvenation and memory

An even more interesting behaviour appears when the temperature is made to vary with time. In fact, we shall consider here only the simplest protocol for which rejuvenation and memory have been experimentally found[14] (Fig. 1 (centre) shows our temperature–time scheme). After a relaxation of duration $t_w{}^{\downarrow}$, the temperature is abruptly lowered from the initial temperature $T_1 < T_g$ to a lower temperature T_2 (the choice of T_2 turns out to be critical, as shown below). The system is again allowed to relax at temperature T_2 for an additional time t_w, after which a magnetic field is switched on and the relaxation function S_{ZFC} is measured at times $t_w{}^{\downarrow} + t_w + t$. Surprisingly enough, one finds that the initial relaxation at T_1 has been essentially forgotten: the long-time peak of S_{ZFC} is found at times $t^{eff}{}_H \approx t_w$, which can be substantially shorter than $t_w{}^{\downarrow}$. This is the rejuvenation effect, which was experimentally found more than 20 years ago and which is being reported via a simulation for the first time (Fig. 1, bottom centre), to the best of our knowledge.

Yet, rejuvenation is not the end of the story. After a total time of $t_w{}^{\uparrow} = 2t_w{}^{\downarrow}$, half of it is spent at T_1 and the other half at T_2, and the system is suddenly heated back to the original temperature T_1, where it is left to relax for a time $t_w \ll t_w{}^{\downarrow}$, after which the magnetic field is switched on and the relaxation function is measured. The S_{ZFC} value is found to peak again at $\sim t_w{}^{\downarrow}$, as if the excursion to temperature T_2 never happened (Fig. 1, top right). This is the memory effect, which, at first sight, seems fairly contradictory with the rejuvenation effect.

The physical origin of memory and rejuvenation in spin glasses has not been identified yet. Then, it is perhaps unsurprising that all the past attempts to reproduce these effects in computer simulations have failed[15–20], which has even raised questions about the validity of the standard model of finite-dimensional spin glasses, namely, the Edwards–Anderson model[21,22]. Fortunately, the Janus II dedicated supercomputer[23] has changed this situation, attaining realistic timescales and length scales, as well as allowing—for the first time—a thorough examination of spin-glass dynamics both in the vicinity of critical temperature T_g and in the low-temperature regime.

The spin-glass dynamics at $T < T_g$ comprises the growth of (glassy) magnetic domains of linear size $\xi(t_w)$ (refs. 24–26) (later referred to as ξ_{micro}). The non-equilibrium nature of the process is evident in the growth of $\xi(t_w)$ as t_w varies, which is never ending and extremely slow. In fact, the lower the temperature, the more sluggish is the growth of $\xi(t_w)$ (refs. 7,27). Janus II has reached unprecedentedly large values of $\xi_{micro}(t_w)$, enabling safe extrapolations from the numerical timescale of tenths of a second (when $\xi \approx 20a_0$, where a_0 is the typical spin–spin distance) to the experimental scale of hours[7,27] (when $\xi \approx 200a_0$). This special-purpose computer has also made it possible to simulate[28] the experimental protocol for extracting the spin-glass coherence length from the Zeeman effect[25], thus showing consistency between the Zeeman method and the microscopic approach. Janus II allowed us to perform computer experiments with a native (that is, fixed-temperature or aging) protocol and make a direct comparison of the S_{ZFC} (equation (1)) obtained in the simulation with that from real experiments on a single crystal of CuMn (refs. 9,10,29). The Edwards–Anderson model and CuMn turned out to be governed by the same scaling laws, where ξ is the all-important scaling variable. This agreement between simulations and experiment, however, was established only for native protocols. We need to understand what happens when the temperature is varied.

Experimentalists are prone to attribute the rejuvenation effect to temperature chaos[14] (explanations not invoking temperature chaos have been also proposed[30,31]). Temperature chaos[32–34] is an equilibrium notion stating that spin configurations typical from the Boltzmann distribution at temperature T_1 would be very atypical for temperature T_2, no matter how close T_1 and T_2 are (provided that $T_1, T_2 < T_g$). Temperature chaos could explain why the relaxation at temperature T_1 seems useless at T_2 (that is, rejuvenation). Yet, even in the mean-field approximation, showing that temperature chaos is really present in equilibrium has been a hard task since it is a weak effect[35,36]. Furthermore, extending the equilibrium concept of temperature chaos to the experimentally relevant context of off-equilibrium dynamics is a very recent achievement[37].

Dynamic temperature chaos is spatially extremely heterogeneous (Fig. 2). To measure it, we choose many spheres of linear size R in random positions within the sample. Within each sphere, we compare spin configurations obtained at temperature T_1 and time t_wT_1 with configurations from temperature T_2 and time t_wT_2 (the simplifying choice $\xi(t_wT_1, T_1) = \xi(t_wT_2, T_2) = \xi(t_w)$ was made elsewhere[37]). The comparison is quantitative, through the computation of a correlation coefficient X_{T_1,T_2} (Methods). Many of these spheres turn out to have very weak temperature chaos ($X_{T_1,T_2} \approx 1$). Yet, with low probability, one picks a chaotic sphere with a significantly smaller X_{T_1,T_2}. In fact, the analysis in another work[37] identifies a crossover length scale $\xi^*(T_1, T_2)$: for $\xi(t_w) \ll \xi^*(T_1, T_2)$, chaotic spheres are very rare, but for $\xi(t_w) \gg \xi^*(T_1, T_2)$, chaotic spheres become fairly typical. A scaling law was also found: $\xi^*(T_1, T_2) \propto (T_1 - T_2)^{-1/\zeta_{NE}}$, where $\zeta_{NE} = 1.19(2)$.

Our last building block comes from the experiment done in another work[8], which identifies a minimal temperature jump ΔT_{min} in a CuMn sample. Temperature chaos in that sample turned out to be exceedingly weak whenever $T_1 - T_2 < \Delta T_{min}$. It follows that in a simulation, chaotic spheres will be just too rare to substantially affect the overall sample relaxation unless (we are indebted to R. Orbach for this observation)

$$\left.\frac{T_1 - T_2}{T_g}\right|_{sim} \approx \left.\frac{\Delta T_{min}}{T_g}\right|_{CuMn}\left[\frac{\xi_{CuMn}(t_w)}{\xi_{micro}(t_w)}\right]^{\zeta_{NE}}, \quad (2)$$

where the subscript micro stands for the ξ value computed in the numerical simulation (Methods), whereas T_g is the glass temperature, which is different for the CuMn sample and for simulations. Plugging in typical numbers ($\Delta T_{min} = 450$ mK, $T_g = 31.5$ K, $\xi_{CuMn}(t_w) \approx 220a_0$ and $\xi_{micro}(t_w) \approx 16.6a_0$), we conclude from equation (2) that given the correlation length reached in our simulations, a successful simulation of the rejuvenation effect should have $T_1 - T_2 > 0.32T_g$.

In this work, we have considered two temperature jumps (Table 1). The first jump, namely, $T_1 = 0.9 \to T_2 = 0.5$, meets the requirement for temperature chaos expressed in equation (2), whereas the second jump, namely, $T_1 = 0.9 \to T_2 = 0.7$, is too small. Hence, we expect to find qualitative differences between the two.

Becoming quantitative: how many controlling length scales?

Our discussion shall emphasize three different length scales, focusing on their physical interpretation and their utility to rationalize

https://doi.org/10.1038/s41567-023-02014-6

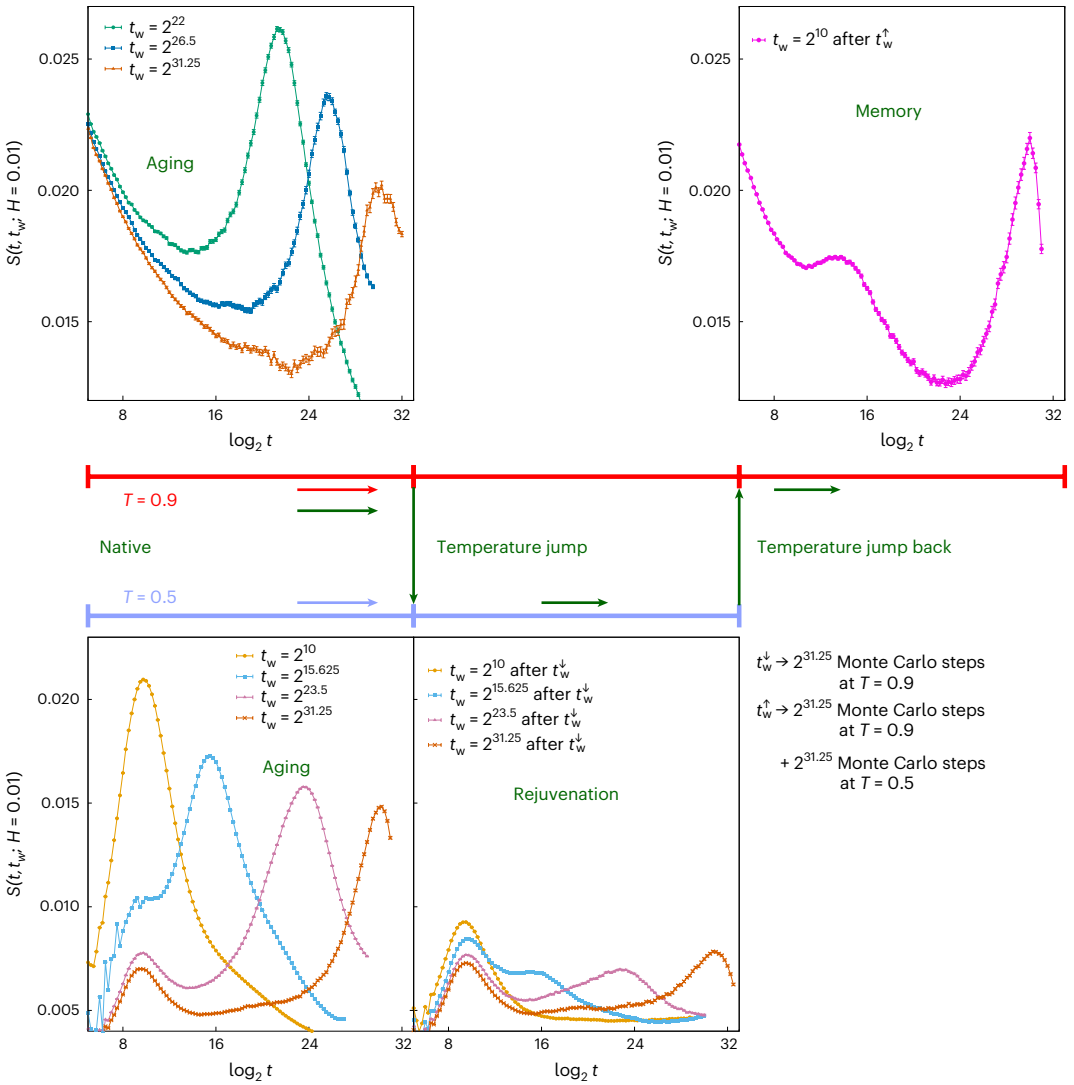

Fig. 1 | ZFC numerical experiment measuring rejuvenation and memory. The starting random spin configuration is instantaneously placed at the working temperature and it relaxes for time t_w without a field. At time t_w, magnetic field $H = 0.01$ is applied and the magnetic density $M_{ZFC}(t, t_w; H)$ is recorded. The left panels show aging. We display the relaxation function $S_{ZFC}(t, t_w; H)$ (equation (1)) for the native runs at the warmer ($T_1 = 0.9$) and colder ($T_2 = 0.5$) temperatures (both below the glass temperature $T_g = 1.102(3)$ (ref. 42)). The physically interesting peak of $S_{ZFC}(t, t_w; H)$ defines $t^{eff}_H \simeq t_w$ (the peak at shorter times, $t \approx 2^{10}$, does not change with the waiting time, which makes this peak uninteresting for us; Methods). In our protocol (indicated by the green arrows), after a waiting time of $t_w^{\downarrow} = 2^{31.25}$, the temperature abruptly drops from the initial temperature ($T_1 = 0.9$) to the colder temperature ($T_2 = 0.5$). Then, the system relaxes at T_2 for an additional time, after which the magnetic field is switched on and the function $S_{ZFC}(t, t_w; H)$ (bottom centre) is measured. Waiting times for these jump runs are reported in the legend; the rejuvenation effect is clearly visible, since $t^{eff}_H \ll t_w^{\downarrow}$ and similar to time t_w spent at T_2 (we use t_w for the time spent at the last temperature in a given protocol). Finally, after waiting time $t_w^{\uparrow} = 2t_w^{\downarrow} = 2^{32.25}$ (that is, the system has spent half of its life at the initial temperature T_1 and the other half at the colder temperature T_2 without a field), the spin glass is suddenly heated back to T_1. We let the system relax for a short time, $t_w = 2^{10} \ll t_w^{\downarrow}$, after which the magnetic field is switched on. The $S_{ZFC}(t, t_w; H)$ measured after the jump back (top right) has a peak very similar to the one before the first jump (top left), evincing the memory of aging at initial temperature T_1, notwithstanding the rejuvenation observed when staying at lower temperature T_2. In Table 1, we report the effective times $t^{eff}_{H=0.01}$ (that is, the time at which the aging peak is found). In all the cases, the error bars are computed with a jack-knife method applied to the 512 replicas that we simulate for every sample. Data are presented as mean values ± standard error of the mean.

the rejuvenation and memory effects (extra details are provided in Methods). Only one of these scales, namely, ξ_{Zeeman}, can be experimentally accessed nowadays (the other two lengths, however, provide invaluable microscopic information):

- ξ_{micro} is the size of the (glassy) domains within the sample (it is the largest length scale at which we can regard the system as ordered at time t_w).
- ξ_{Zeeman} is obtained by counting the number of spins that coherently react to an externally applied field[25]. It provides a very direct quantification of memory and rejuvenation.
- $\zeta(t_1, t_2)$ (refs. 38–40) is obtained from a comparison of the same system at two times t_1 and t_2 ($t_1 < t_2$): ζ characterizes the long-distance decay of the pair-correlation function corresponding to the set of spins taking opposite signs at times t_1 and t_2 (Methods) (physically, $\zeta(t_1, t_2)$ is the typical size of regions where coherent rearrangements have occurred between times t_1 and t_2, probably because of the ongoing formation of a new spin order at time t_2). For fixed t_1, $\zeta(t_1, t_2)$ grows with t_2 starting from $\zeta(t_1, t_2 = t_1) = 0$.

Previous analysis for native (that is, fixed-temperature) protocols tell us that ξ_{Zeeman} fairly closely follows the behaviour of microscopic

https://doi.org/10.1038/s41567-023-02014-6

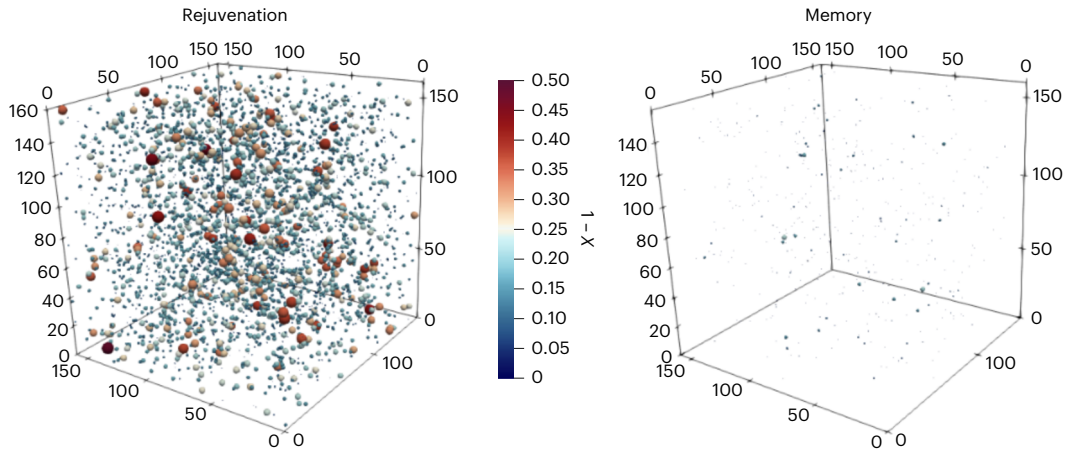

Fig. 2 | Temperature chaos is spatially heterogeneous when it is clearly present. Rejuvenation protocol (left) and memory protocol (right). The 8,000 randomly chosen spheres in a sample of size $L = 160$ are depicted with a colour code depending on $1–X$ (X is the chaotic correlation parameter as computed for spheres with radius $R = 5a_0$; Methods). For visualization purposes, spheres are represented with a radius of $12(1–X)$, so that only fully chaotic spheres (that is, $X = 0$) would have the largest size. To avoid cluttering, we draw only spheres with $X < 0.97$. We calculate the chaotic correlation parameter X (left) between the native system at $T = 0.5$ (that is, a fixed-temperature protocol: a completely disordered system is put at temperature $T = 0.5$ and let to evolve at this temperature for a time $t_w = 2^{31.25}$) and the jump system at the same temperature $T = 0.5$ (Fig. 1 (centre): the jump system has spent the first half of its life, $t_w^{\downarrow} = 2^{31.25}$, at the hot temperature $T_1 = 0.9$ and the second half, $t_w = 2^{31.25}$, at the cold temperature $T = 0.5$). Very strong chaotic heterogeneity is found. We calculate the chaotic correlation parameter X (right) between the native system at the hot temperature $T = 0.9$ and the jump-back system at the same temperature $T = 0.9$ (the jump-back system has spent a time $t_w^{\downarrow} = 2^{31.25}$ at the hot temperature $T_1 = 0.9$, a time $t_w^{\uparrow} - t_w^{\downarrow} = 2^{31.25}$ at the cold temperature $T_2 = 0.5$, and then $t_w = 2^{10}$ again at $T_1 = 0.9$; Fig. 1 shows the temperature protocol). After the cycle, the system does not display chaotic heterogeneity since almost every sphere has a large correlation parameter X, that is, a strong memory (Supplementary Note V provides more examples).

Table 1 | Basic features of our simulations

Type	T	(History) + t_w	$\xi_{micro}(t_w)$	$\xi_{Zeeman}(t_w)$	$\zeta(t_w, 2t_w)$	$\log_2 t^{eff}{}_{H=0.01}$	t_{max}
Native (aging)	0.9	$2^{31.25}$	16.63(5)	16.64(5)		29.66(2)	2^{32}
Native (aging)	0.5	2^{10}	2.23926(2)		1.916(1)	9.813(1)	2^{28}
Native (aging)	0.5	$2^{15.625}$	2.9090(4)		2.571(4)	15.377(2)	2^{28}
Native (aging)	0.5	$2^{23.5}$	4.0865(15)	3.5175(2)	3.77(1)	22.942(4)	2^{30}
Native (aging)	0.5	$2^{31.25}$	5.6167(4)	5.617(4)	5.30(4)	29.500(8)	2^{32}
Native (rejuv)	0.5	($2^{31.25}$ at T=0.9)+2^{10}	16.62(12)	2.43(2)	1.488(3)	19.016(7)	2^{28}
Native (rejuv)	0.5	($2^{31.25}$ at T=0.9)+$2^{15.625}$	16.68(12)	3.67(1)	1.869(2)	22.156(8)	2^{28}
Native (rejuv)	0.5	($2^{31.25}$ at T=0.9)+$2^{23.5}$	16.75(13)	4.83(8)	2.69(1)	26.699(9)	2^{31}
Native (rejuv)	0.5	($2^{31.25}$ at T=0.9)+$2^{31.25}$	16.81(13)	6.43(8)	3.958(9)	31.56(1)	$2^{33.5}$
Native (aging)	0.7	2^{10}	2.6629(4)		2.054(1)	9.948(1)	2^{28}
Native (aging)	0.7	$2^{15.625}$	3.8230(10)		2.931(4)	15.502(3)	2^{28}
Native (aging)	0.7	$2^{23.5}$	6.1742(4)	5.50(1)	4.72(4)	23.042(6)	2^{28}
Native (aging)	0.7	$2^{31.25}$	9.578(11)	9.578(1)	7.50(1)	30.39(1)	2^{33}
Native (rejuv)	0.7	($2^{31.25}$ at T=0.9)+2^{10}	16.62(12)	6.59(7)	1.652(3)	23.08(1)	2^{28}
Native (rejuv)	0.7	($2^{31.25}$ at T=0.9)+$2^{15.625}$	16.67(12)	7.61(8)	2.194(5)	24.48(1)	2^{28}
Native (rejuv)	0.7	($2^{31.25}$ at T=0.9)+$2^{23.5}$	16.76(12)	9.26(10)	3.43(4)	26.82(2)	2^{28}
Native (rejuv)	0.7	($2^{31.25}$ at T=0.9)+$2^{31.25}$	16.81(13)	12.12(1)	5.59(9)	29.40(2)	2^{32}
Jump back (memory)	0.9	$\begin{pmatrix} 2^{31.25} \text{ at } T=0.9 \\ 2^{31.25} \text{ at } T=0.5 \end{pmatrix} + 2^{10}$	16.81(13)	16.05(2)	1.812(3)	29.98(2)	2^{32}

The runs labelled as native are intended for the study of aging, those labelled as jump are devoted to rejuvenation, and those labelled jump-back are for memory (see the definitions given later). On the Janus II supercomputer, we have simulated the Edwards–Anderson model with nearest-neighbour couplings (J=±1 with 50% probability), comprising simple-cubic lattices containing 1,603 Ising spins s=±1 (lattice size, L=160a_0) and endowed with periodic boundary conditions. A particular set of couplings is termed a sample. For every sample and every set of parameters, we have simulated 512 independent trajectories (that is, 512 replicas; Methods). This table lists the main parameters for each of our numerical simulations. Temperature-varying protocols (Fig. 1, centre and top right) are termed the jump and jump-back protocols, respectively. In all these cases, temperature T refers to the temperature at which the relaxation function in equation (1) is computed. All the temperatures considered here are in the spin-glass phase: $T < T_g$=1.102(3) (ref. 42). The waiting time is the time elapsed at the working temperature before magnetic field H is switched on (for native protocols, this consists of time t_w at working temperature T; for jump protocols, the system stays for time $t_w^{\downarrow}$ at starting temperature T_1=0.9 plus time t_w at T_2; for the jump-back protocols, the system stays for time $t_w^{\downarrow}$ at starting temperature T_1=0.9, plus time $t_w^{\uparrow}$ at cold temperature T_2=0.5, plus short time t=210 back at temperature T_1). The three length scales characterizing the dynamics, namely, ξ_{micro}, ξ_{Zeeman} and $\zeta(t_1=t_w, t_2=2t_w)$ are given in a_0=1 unit (Methods; $\zeta(t_1, t_2)$ is calculated in the absence of an external magnetic field, ξ_{micro} is computed just before the magnetic field is switched on and ξ_{Zeeman} reflects the dependence of relaxation rate S_{ZFC} on the magnetic field; equation (1)). We incur a slight language abuse when writing $\zeta(t_1=t_w, t_2=2t_w)$, which is only accurate for native runs. For the jump runs, it is $t_1=t_w^{\downarrow}+t_w$ ($t_1=t_w^{\downarrow}+t_w^{\uparrow}+t_w$ for jump-back protocols). In all the cases, we have $t_2=t_1+t_w$. Finally, we report t_{max}, our longest simulation time in the presence of a field, and the effective time $t^{eff}{}_H$, the time of the aging peak of the relaxation function (as computed for field H=0.01; Fig. 1 and Methods). In all the cases, the error bars denote one standard deviation

https://doi.org/10.1038/s41567-023-02014-6

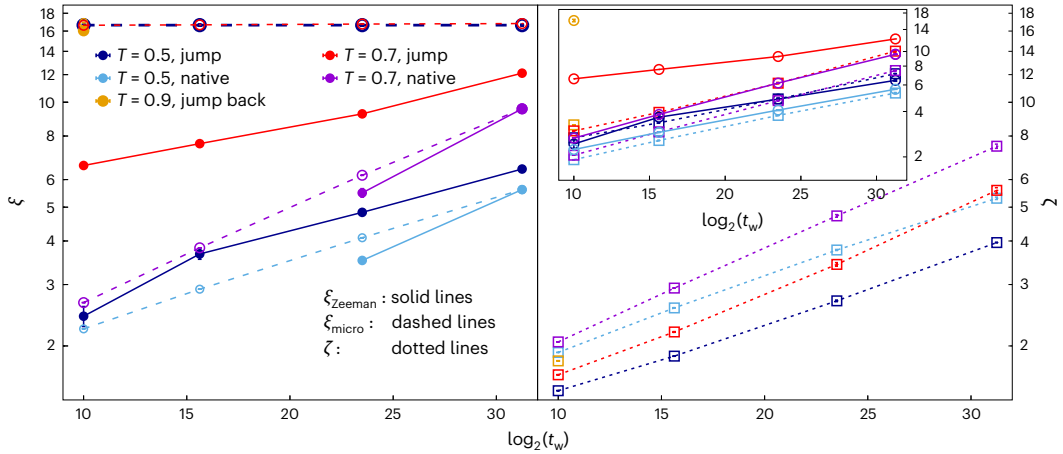

Fig. 3 | Aging dynamics is controlled by at least three length scales. The main text and Methods provide an extended discussion on the three length scales. The solid lines and filled circles denote $\xi_{\mathrm{Zeeman}}(t_w, T)$, the dashed lines and empty circles denote $\xi_{\mathrm{micro}}(t_w, T)$, and the dotted lines and empty squares denote $\zeta(t_1, t_2)$. For the native protocols (left), $\xi_{\mathrm{Zeeman}}(t_w)$ fairly closely follows the behaviour of $\xi_{\mathrm{micro}}(t_w)$. For the jump protocol with $T_2 = 0.5$, $\xi_{\mathrm{Zeeman}}(t_w)$ is extremely similar to the corresponding curve for the native run (this T_2 value meets the chaos requirement in equation (2)), which means that the system responds to an external magnetic field as if it is rejuvenated, that is, $\xi^{\mathrm{jump}}_{\mathrm{Zeeman}}(t_w) \ll \xi^{\mathrm{jump}}_{\mathrm{micro}}(t_w)$. When the system jumps back to $T_1 = 0.9$ (that is, $T_1 = 0.9 \to T_2 = 0.5 \to T_1 = 0.9$), $\xi^{\mathrm{jump-back}}_{\mathrm{Zeeman}}(t_w)$ goes back to its original value of $\xi^{\mathrm{native}}_{\mathrm{micro}}(t_w)$ after an extremely short time (memory). Instead, $\xi_{\mathrm{Zeeman}}(t_w)$ never becomes small for the jump protocols with $T_2 = 0.7$. The $\xi_{\mathrm{micro}}(t_w)$ value for the jump runs are superimposed (the spins are frozen for this length scale). The size of regions undergoing coherent rearrangements when evolving from the initial to final time, $\zeta(t_1, t_2)$, is much smaller than $\xi_{\mathrm{micro}}(t_w)$ for all our jump protocols (right). The two times at which we evaluate the coherence length, that is, $\zeta(t_1, t_2)$, are $t_1 = t_w$ and $t_2 = 2t_w$ (Table 1 provides a detailed explanation). In all the cases, ζ is represented as a function of $\log_2(t_2 - t_1)$. Supplementary Note III provides extra results on $\zeta(t_1, t_2)$. We compare the behaviour of $\zeta(t_1 = t_w, t_2 = 2t_w)$ and $\xi_{\mathrm{Zeeman}}(t_w)$ (inset). For native runs, the two lengths are approximately equal. Instead, for the jump protocols, we show $1.8\zeta(t_1 = t_w, t_2 = 2t_w)$. Indeed, only for $T_2 = 0.5$ and using an appropriate scaling factor of approximately 2, it is clear that $\zeta^{\mathrm{jump}}(t_1 = t_w, t_2 = 2t_w)$ can be made to coincide with $\xi^{\mathrm{jump}}_{\mathrm{Zeeman}}(t_w)$ (because these curves are approximately parallel in our logarithmic representation). For $T_2 = 0.7$ instead, see the dotted red line in the inset; $\zeta^{\mathrm{jump}}(t_1 = t_w, t_2 = t_w + t_w)$ can be rescaled to coincide with $\xi_{\mathrm{Zeeman}}(t_w)$ from the native protocol (solid violet line), which differs from $\xi^{\mathrm{jump}}_{\mathrm{Zeeman}}(t_w)$ (solid red line). The largest length in this set, $\xi_{\mathrm{Zeeman}}(t_w) \approx 16$, corresponds to the jump-back protocol. Note that for the jump-back protocol, we only have a single point (orange). In all the cases, the error bars are computed with a jack-knife method applied to the four independent samples. Data are presented as mean values ± standard error of the mean.

length ξ_{micro} (refs. 9,10,25,28). This is described in Fig. 3 (left). There are two salient features in the time growth of either ξ_{Zeeman} or $\xi_{\mathrm{micro}}(t_w)$ at a fixed temperature[7,27]: the growth slows down as ξ_{micro} increases ($\mathrm{d}\log t_w/\mathrm{d}\log\xi_{\mathrm{micro}}$ is approximately constant when t_w varies in the logarithmic scale) and the dynamics at lower temperatures is enormously slower ($T\mathrm{d}\log t_w/\mathrm{d}\log\xi_{\mathrm{micro}}$ is roughly constant when different temperatures are compared). In fact, at the largest temperature $T = 0.9$ (Table 1 and ref. 27), it is comparatively easy to reach a large $\xi_{\mathrm{micro}} \approx 16.6a_0$ in the native protocol. Instead, for a similar simulation time, the native protocol at $T = 0.5$ is limited to $\xi_{\mathrm{micro}} \approx 5.6a_0$. It is then unsurprising that when the temperature jumps from $T_1 = 0.9$ to $T_2 = 0.5$ or 0.7 (Fig. 3, left), the size of the glassy domains is locked to their value at jump time, namely, $\xi_{\mathrm{micro}} \approx 16.6a_0$: the time needed for such a large domain to grow at a lower temperature T_2 far exceeds the scale of our simulations. The importance of this locking was also emphasized elsewhere[17].

Although ξ_{micro} is locked at the value that it has at jump time, the behaviour of ξ_{Zeeman} is different in the jump protocols. In the jump complying with equation (2), $T_1 = 0.9 \to T_2 = 0.5$, $\xi_{\mathrm{Zeeman}}(t_w)$ is fairly similar to the corresponding curve for the native run at $T = 0.5$. From the point of view of the response to a magnetic field, rejuvenation is almost complete for this temperature jump, because the initial relaxation at $T_1 = 0.9$ (almost) does not leave a measurable trace. Instead, for the more modest jump $T_1 = 0.9 \to T_2 = 0.7$, rejuvenation is weaker and ξ_{Zeeman} is sensibly larger than in the native runs (Supplementary Note II).

Furthermore, it is also shown in Fig. 3 (left) that when the system jumps back to $T_1 = 0.9$ (that is, $T_1 = 0.9 \to T_2 = 0.5 \to T_1 = 0.9$; Fig. 1 (top right)), the response to the magnetic field goes back to normal: ξ_{Zeeman} catches up with ξ_{micro} after an extremely short transient. This is another manifestation of the memory effect.

With regard to the third length scale (Fig. 3 (right) and Supplementary Note III), for all our jump protocols, we find $\zeta \ll \xi_{\mathrm{micro}}$, which means that the configuration right before the jump is only locally distorted by the excursion to low temperature T_2 (in our opinion, this fact provides a natural explanation for the memory effect). Figure 3 (inset) shows that ζ is not just a simple function of ξ_{micro} and ξ_{Zeeman}. The consequences of this sophisticated behaviour are discussed below.

Dynamic temperature chaos and rejuvenation

At this point, the elephant in the room is clear: what is the physical origin for rejuvenation and memory?

To answer the question, we need to compare pairs of spin configurations. One of the configurations will be taken from the jump protocols. The other configuration will come from the native runs at temperatures $T_2 = 0.5$ or $T_2 = 0.7$. In an attempt to make a fair comparison, we shall choose the native configurations at T_2 at their largest possible waiting time. In fact, the magnetic domains will be substantially smaller in the native protocol than those in the jump protocol (at $T_2 = 0.5$, for instance, one has to compare $\xi^{\mathrm{native}}_{\mathrm{micro}} \approx 5.8a_0$ with $\xi^{\mathrm{jump}}_{\mathrm{micro}} \approx 16.6a_0$).

The main steps in the comparison were outlined above (Methods and ref. 37). At random in the sample, we pick spheres of radius R. The results presented in this paper were obtained with $R = 5a_0$ to make sure that the spheres will have a chance to fit within the glassy domains of the native runs (we have tried other values of R, finding qualitatively similar results; Supplementary Note VI). The configurations from the two protocols are compared by computing a correlation coefficient X that only takes into account spins contained in the sphere. If X is significantly smaller than unity, we regard that particular sphere as chaotic, because typical configurations from the two protocols differ within the sphere. To be precise, we compute the probability distribution function $F(\tilde{X})$, namely, the fraction of the spheres with a correlation coefficient $X < \tilde{X}$.

https://doi.org/10.1038/s41567-023-02014-6

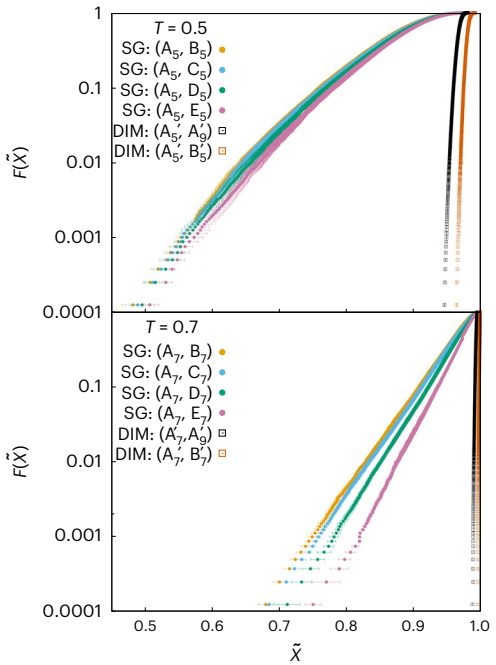

Fig. 4 | Strong temperature chaos correlates with full rejuvenation. Here we show the fraction of spheres with radius $R = 5a_0$ that have correlation parameter X smaller than $\tilde{X}$, $F(\tilde{X})$ (Methods; the pairs of systems for which correlation parameter X is computed are listed in Table 2). One of the systems in the pair used to compute X is always taken from the native protocol at $T = 0.5$ (top) ($T = 0.7$ (bottom)). In the cases reported in the top panel, the partner in the pair that undergoes the temperature-jump protocol experiences strong rejuvenation. Instead, as shown in Fig. 3 (left), rejuvenation is only partial for the cases reported in the bottom panel. Interestingly enough, small correlation parameters appear with high probability in the top panel, whereas they are very rare events in the bottom panel. We also show a comparison with the DIM (Methods describes our null experiment), where temperature chaos is not expected. Indeed, in the absence of temperature chaos, the probability concentrates at $X \approx 1$. In all the cases, the error bars are computed with a jack-knife method applied to the 512 replicas that we simulate for every sample. Data are presented as mean values ± standard error of the mean.

Our results (Fig. 4 (bottom)) for the jump protocol $T_1 = 0.9 \to T_2 = 0.7$ remind us of previous studies[37]. The vast majority of spheres have a very large correlation coefficient, and truly chaotic spheres are only found in the tail of the distribution (probability of 0.1% or smaller).

Interestingly enough (Fig. 2 (left) and Fig. 4 (top)), the situation is radically different for the jump protocol $T_1 = 0.9 \to T_2 = 0.5$, where the spheres in the tenth percentile of the distribution are as chaotic as the most chaotic spheres we could find for the jump $T_1 = 0.9 \to T_2 = 0.7$. In fact, to the best of our knowledge, Fig. 4 (top) reports the strongest temperature-chaos signal ever observed in a simulation of glassy dynamics.

To convince ourselves that the extreme chaos is not an artefact of the disparity in domain sizes, we have tried a null experiment by simulating a model where no temperature chaos is expected, namely, the link-diluted ferromagnetic Ising model (we used the results from another work[41] to as closely match as possible the conditions in our spin-glass simulations with the diluted ferromagnet, taking special care in matching the size of the domains; Methods). As expected (Fig. 4), the sphere distribution for the ferromagnet is concentrated at correlation coefficient $X \approx 1$. We conclude that the spin-glass results (Fig. 4 (top)) are genuine evidence for dynamic temperature chaos.

It is also interesting that the distribution function (Fig. 4 (top)) barely depends on t_w. This is another manifestation of the dynamic lockdown when the temperature jumps to the lower value.

Table 2 | Identifying parameters for each numerical simulation in Fig. 4

	System	T	Type	Waiting time
A_9	SG	0.9	Native	$t_w^{\downarrow}=2^{31.25}$
B_9	SG	0.9	Jump back	$t_w^{\downarrow}+t_w^{\uparrow}+2^{10}$
A_5	SG	0.5	Native	$t_w^{\downarrow}=2^{31.25}$
B_5	SG	0.5	Native	$t_w^{\downarrow}=2^{10}$
C_5	SG	0.5	Native	$t_w^{\downarrow}=2^{15.625}$
D_5	SG	0.5	Native	$t_w^{\downarrow}=2^{23.5}$
E_5	SG	0.5	Native	$t_w^{\downarrow}=2^{31.25}$
A_7	SG	0.7	Native	$t_w^{\downarrow}=2^{31.25}$
B_7	SG	0.7	Native	$t_w^{\downarrow}=2^{10}$
C_7	SG	0.7	Native	$t_w^{\downarrow}=2^{15.625}$
D_7	SG	0.7	Native	$t_w^{\downarrow}=2^{23.5}$
E_7	SG	0.7	Native	$t_w^{\downarrow}=2^{31.25}$
A'_5	DIM	0.5	Native	76
B'_5	DIM	0.5	Native	430+69
A'_7	DIM	0.7	Native	197
B'_7	DIM	0.7	Native	430+165
A'_9	DIM	0.9	Native	430

Spin-glass (SG) protocols follow the notation shown in Fig. 1. T is the final temperature in the protocol. For DIM (Method s shows the DIM temperature-naming convention), we explicitly write $t_w^{(1)}+t_w^{(2)}$ for the jump protocols to stress that the time before the jump (T=0.9), that is, $t_w^{(1)}$, differs from time $t_w^{(2)}$ at the final temperature. We choose $t_w^{(1)}$ such that ξ_{micro} coincides for both protocols in the pairs (A_5, A'_5), (A_7, A'_7) and (A_9, A'_9).

The overall conclusions of this analysis are twofold. First, the requirement expressed by equation (2), which is based on CuMn experimental results[8], is sensible: strong temperature chaos is found only when $T_1 - T_2$ is as large as equation (2) demands. Second, only when the temperature chaos is strong, our simulations find strong rejuvenation (Fig. 3 (left)).

Where do we stand?

Our simulations depict a clear picture of rejuvenation and memory effects. Provided that the temperature jump is large enough (equation (2)), the spin-glass state that was forming at temperature T_1 is completely alien at temperature T_2 (at least, it looks alien compared with the native state that grows directly at T_2; Fig. 2). In fact, the response to the magnetic field (which is the quantity measured in the experiments[2–5,7–10,14]) is not qualitatively different in the alien state and in the native state that grows from a fully disordered high-temperature state. The system just dismisses the relaxation it achieved at the higher temperature T_1.

Paradoxically enough, the alien state is locked at temperature T_2: the microscopic rearrangement at T_2 (Fig. 3 (right)), takes place on extremely small length scales to dissolve such foreign glassy domains. As a consequence, when the temperature is taken back to T_1, the glassy domains characteristic of T_1 are still there. This seems to be the physical origin of the memory effect. This reasoning is also consistent with recent experiments that find that the memory effect strongly depends on $t_w^{\downarrow}$ (that is, the time spent in the first stay at T_1) (J. Freedberg, personal communication). Indeed, if $t_w^{\downarrow}$ is too small, the memory effect almost disappears. Our interpretation of this experimental finding is that the glassy domains at T_1 need to grow large enough as to remain mostly unaltered at the lower temperature T_2.

Looking back, we effectively understand why rejuvenation has been so difficult to find in simulations: the correlation lengths that could be reached before the Janus family of supercomputers were rather limited (we are referring here to the ξ_{micro} length scale).

Therefore, equation (2) would demand an exceedingly large temperature jump $T_1 - T_2$ if one wants to have a large fraction of chaotic spheres of the relevant size.

An open question is whether or not the only experimentally accessible coherence length, namely, $\xi_{\mathrm{Zeeman}}(t_w)$, relates to some correlation function under all the circumstances. Indeed, in the case of native protocols, $\xi_{\mathrm{Zeeman}}(t_w)$ behaves analogous to $\xi_{\mathrm{micro}}(t_w)$, which we know how to obtain from a microscopic correlation function. However, $\xi_{\mathrm{micro}}(t_w)$ is not a valid proxy for $\xi_{\mathrm{Zeeman}}(t_w)$ in temperature-jump protocols. Fortunately (Fig. 3 (inset)), we achieve a step forward in this respect (but only if temperature chaos is strong enough). Indeed, if the condition in equation (2) is met, we have found that it is possible to rescale $\zeta(t_1 = t_w, t_2 = t_w + t_w)$ in such a way that it coincides with $\xi_{\mathrm{Zeeman}}(t_w)$, with a scaling factor in the range between 1 and 2. In other words, we are extending the main result of another work[28] to jump protocols (because $\zeta(t_1 = t_w, t_2 = t_w + t_w)$ basically coincides with $\xi_{\mathrm{micro}}(t_w)$ for native protocols). Hence, our data suggest that ζ may help us bridge the microscopic world in a more complete way, namely, the correlation functions that we compute in a simulation (Methods provides the definition of ζ), with the macroscopic world of the response to an external field (quantified by ξ_{Zeeman}).

Finally, we should also stress that the analysis of the rejuvenation and memory effects requires the consideration of at least three different length scales, namely, $\xi_{\mathrm{micro}}(t_w)$, $\xi_{\mathrm{Zeeman}}(t_w)$ and $\zeta(t_1, t_2)$, which can be fairly different from each other. Of course, one of these three, namely, the domain size $\xi_{\mathrm{micro}}(t_w)$, acts as a cut-off for the other lengths. Yet, we have seen that $\xi_{\mathrm{micro}}(t_w)$ is not nearly enough to describe the variety of behaviours that an aging system may present. In fact, $\xi_{\mathrm{micro}}(t_w)$ has stayed essentially constant for all the jump simulations that we have considered here. Therefore, a useful theory of aging dynamics cannot feature only a single length scale. In this sense, we think that our work poses a new and noteworthy question for the different theories of aging dynamics.

Online content

Any methods, additional references, Nature Portfolio reporting summaries, source data, extended data, supplementary information, acknowledgements, peer review information; details of author contributions and competing interests; and statements of data and code availability are available at https://doi.org/10.1038/s41567-023-02014-6.

References

1. Struik, C. L. E. *Physical Aging in Amorphous Polymers and Other Materials* (Elsevier, 1980).
2. Jonason, K., Vincent, E., Hammann, J., Bouchaud, J. P. & Nordblad, P. Memory and chaos effects in spin glasses. *Phys. Rev. Lett.* **81**, 3243–3246 (1998).
3. Lundgren, L., Svedlindh, P. & Beckman, O. Anomalous time dependence of the susceptibility in a Cu(Mn) spin glass. *J. Magn. Magn. Mater.* **31–34**, 1349–1350 (1983).
4. Jonsson, T., Jonason, K., Jönsson, P. E. & Nordblad, P. Nonequilibrium dynamics in a three-dimensional spin glass. *Phys. Rev. B* **59**, 8770 (1999).
5. Hammann, J. et al. Comparative review of aging properties in spin glasses and other disordered materials. *J. Phys. Soc. Jpn* **Supplement A**, 206–211 (2000).
6. Mydosh, J. A. *Spin Glasses: An Experimental Introduction* (Taylor and Francis, 1993).
7. Zhai, Q., Martin-Mayor, V., Schlagel, D. L., Kenning, G. G. & Orbach, R. L. Slowing down of spin glass correlation length growth: simulations meet experiments. *Phys. Rev. B* **100**, 094202 (2019).
8. Zhai, Q., Orbach, R. L. & Schlagel, D. L. Evidence for temperature chaos in spin glasses. *Phys. Rev. B* **105**, 014434 (2022).
9. Zhai, Q. et al. Scaling law describes the spin-glass response in theory, experiments, and simulations. *Phys. Rev. Lett.* **125**, 237202 (2020).
10. Paga, I. et al. Spin-glass dynamics in the presence of a magnetic field: exploration of microscopic properties. *J. Stat. Mech.* **2021**, 033301 (2021).
11. Albert, S. et al. Fifth-order susceptibility unveils growth of thermodynamic amorphous order in glass-formers. *Science* **352**, 1308–1311 (2016).
12. Mézard, M., Parisi, G. & Virasoro, M. *Spin-Glass Theory and Beyond* (World Scientific, 1987).
13. Vincent, E., Hammann, J., Ocio, M., Bouchaud, J.-P. & Cugliandolo, L. F. Slow dynamics and aging in spin glasses in complex behavior of glassy systems (eds Rubí, M. & Pérez-Vicente, C.) 492 (Springer, 1997).
14. Djurberg, C., Jonason, K. & Nordblad, P. Magnetic relaxation phenomena in a CuMn spin glass. *Eur. Phys. J. B* **10**, 15–21 (1999).
15. Komori, T., Yoshino, H. & Takayama, H. Numerical study on aging dynamics in the 3D Ising spin-glass model. II. Quasi-equilibrium regime of spin auto-correlation function. *J. Phys. Soc. Jpn* **69**, 1192–1201 (2000).
16. Picco, M., Ricci-Tersenghi, F. & Ritort, F. Chaotic, memory, and cooling rate effects in spin glasses: evaluation of the Edwards-Anderson model. *Phys. Rev. B* **63**, 174412 (2001).
17. Berthier, L. & Bouchaud, J.-P. Geometrical aspects of aging and rejuvenation in the Ising spin glass: a numerical study. *Phys. Rev. B* **66**, 054404 (2002).
18. Takayama, H. & Hukushima, K. Numerical study on aging dynamics in the 3D Ising spin–glass model: III. Cumulative memory and 'chaos' effects in the temperature-shift protocol. *J. Phys. Soc. Jpn* **71**, 3003–3010 (2002).
19. Maiorano, A., Marinari, E. & Ricci-Tersenghi, F. Edwards-Anderson spin glasses undergo simple cumulative aging. *Phys. Rev. B* **72**, 104411 (2005).
20. Jiménez, S., Martín-Mayor, V. & Pérez-Gaviro, S. Rejuvenation and memory in model spin glasses in three and four dimensions. *Phys. Rev. B* **72**, 054417 (2005).
21. Edwards, S. F. & Anderson, P. W. Theory of spin glasses. *J. Phys. F: Met. Phys.* **5**, 965 (1975).
22. Edwards, S. F. & Anderson, P. W. Theory of spin glasses. II. *J. Phys. F: Met. Phys.* **6**, 1927 (1976).
23. Baity-Jesi, M. et al. Janus II: a new generation application-driven computer for spin-system simulations. *Comp. Phys. Comm* **185**, 550–559 (2014).
24. Marinari, E., Parisi, G., Ruiz-Lorenzo, J. & Ritort, F. Numerical evidence for spontaneously broken replica symmetry in 3D spin glasses. *Phys. Rev. Lett.* **76**, 843–846 (1996).
25. Joh, Y. G., Orbach, R., Wood, G. G., Hammann, J. & Vincent, E. Extraction of the spin glass correlation length. *Phys. Rev. Lett.* **82**, 438–441 (1999).
26. Belletti, F. et al. Nonequilibrium spin-glass dynamics from picoseconds to one tenth of a second. *Phys. Rev. Lett.* **101**, 157201 (2008).
27. Baity-Jesi, M. et al. Aging rate of spin glasses from simulations matches experiments. *Phys. Rev. Lett.* **120**, 267203 (2018).
28. Baity-Jesi, M. et al. Matching microscopic and macroscopic responses in glasses. *Phys. Rev. Lett.* **118**, 157202 (2017).
29. Paga, I. et al. Magnetic-field symmetry breaking in spin glasses. Preprint at https://arxiv.org/abs/2207.10640 (2022).
30. Cugliandolo, L. F. & Kurchan, J. Mean-field theory of temperature cycling experiments in spin glasses. *Phys. Rev. B* **60**, 922–930 (1999).
31. Berthier, L. & Bouchaud, J.-P. Comment on 'symmetrical temperature-chaos effect with positive and negative temperature shifts in a spin glass'. *Phys. Rev. Lett* **90**, 059701 (2003).
32. McKay, S. R., Berker, A. N. & Kirkpatrick, S. Spin-glass behavior in frustrated Ising models with chaotic renormalization-group trajectories. *Phys. Rev. Lett.* **48**, 767–770 (1982).
33. Bray, A. J. & Moore, M. A. Chaotic nature of the spin-glass phase. *Phys. Rev. Lett.* **58**, 57–60 (1987).

34. Kondor, I. On chaos in spin glasses. *J. Phys. A: Math. Gen.* **22**, L163 (1989).
35. Rizzo, T. & Crisanti, A. Chaos in temperature in the Sherrington-Kirkpatrick model. *Phys. Rev. Lett.* **90**, 137201 (2003).
36. Parisi, G. & Rizzo, T. Chaos in temperature in diluted mean-field spin-glass. *J. Phys. A: Math. Theor.* **43**, 235003 (2010).
37. Baity-Jesi, M. et al. Temperature chaos is present in off-equilibrium spin-glass dynamics. *Commun. Phys.* **4**, 74 (2021).
38. Belletti, F. et al. An in-depth look at the microscopic dynamics of Ising spin glasses at fixed temperature. *J. Stat. Phys.* **135**, 1121–1158 (2009).
39. Castillo, H. E., Chamon, C., Cugliandolo, L. F. & Kennett, M. P. Heterogeneous aging in spin glasses. *Phys. Rev. Lett.* **88**, 237201 (2002).
40. Jaubert, L. C., Chamon, C., Cugliandolo, L. F. & Picco, M. Growing dynamical length, scaling, and heterogeneities in the 3D Edwards-Anderson model. *J. Stat. Mech.* **2007**, P05001 (2007).
41. Berche, P.-E., Chatelain, C., Berche, B. & Janke, W. Bond dilution in the 3D Ising model: a Monte Carlo study. *Eur. Phys. J. B* **38**, 463–474 (2004).
42. Baity-Jesi, M. et al. Critical parameters of the three-dimensional Ising spin glass. *Phys. Rev. B* **88**, 224416 (2013).

[1]Eawag, Überlandstrasse 133, Dübendorf, Switzerland. [2]Dipartimento di Fisica e Scienze della Terra, Università di Ferrara and INFN, Ferrara, Italy. [3]Departamento de Física Teórica, Universidad de Zaragoza, Zaragoza, Spain. [4]Instituto de Biocomputación y Física de Sistemas Complejos (BIFI), Zaragoza, Spain. [5]Departamento de Física Teórica, Universidad Complutense, Madrid, Spain. [6]Departamento de Ingeniería Eléctrica, Electrónica y Automática, Universidad de Extremadura, Cáceres, Spain. [7]Instituto de Computación Científica Avanzada (ICCAEx), Universidad de Extremadura, Badajoz, Spain. [8]Fundación ARAID, Diputación General de Aragón, Zaragoza, Spain. [9]Dipartimento di Biotecnologie, Chimica e Farmacia, Università degli Studi di Siena, Siena, Italy. [10]Dipartimento di Fisica, Sapienza Università di Roma, Rome, Italy. [11]CNR-Nanotec, Rome Unit, Rome, Italy. [12]INFN, Sezione di Roma, Rome, Italy. [13]Departamento de Física, Universidad de Extremadura, Badajoz, Spain. [14]Departamento de Ingeniería Electrónica y Comunicaciones and I3A, Universidad de Zaragoza, Zaragoza, Spain. [15]Institute of Nanotechnology, Soft and Living Matter Laboratory, Consiglio Nazionale delle Ricerche (CNR-NANOTEC), Rome, Italy. [16]Dipartimento di Scienze Chimiche e Farmaceutiche, Università di Ferrara e INFN Sezione di Ferrara, Ferrara, Italy. [17]Université Paris-Saclay, CNRS, INRIA Tau team, LISN, Gif-sur-Yvette, France. [18]Chan Zuckerberg Biohub, San Francisco, CA, USA. ✉e-mail: ilaria.paga@gmail.com

Methods

The layout of this note is as follows. First, we describe our simulations. Then, we define some quantities characteristic of the ZFC protocol. In fact, the magnetic field plays a crucial role in the determination of the Zeeman length scale, as explained thereafter. The other two spin-glass coherence lengths, ξ_{micro} and ζ, are computed later. Finally, we explain our computation of the chaotic correlation parameter.

Simulated models

We performed massive simulations on the Janus II supercomputer[23] to study the three-dimensional Edwards–Anderson model on a cubic lattice with periodic boundary conditions and size $L = 160$ (in units of lattice constant a_0). The main parameters describing our simulations are provided in Table 1.

The $N = L^3$ Ising spins, $s_{\mathbf{x}} = \pm 1$, interact with their lattice nearest neighbours in the presence of a magnetic field (H) through the Hamiltonian:

$$\mathcal{H} = -\sum_{\langle \mathbf{x},\mathbf{y}\rangle} J_{\mathbf{xy}} s_{\mathbf{x}} s_{\mathbf{y}} - H\sum_{\mathbf{x}} s_{\mathbf{x}}, \tag{3}$$

where the couplings are independent, identically distributed random variables: $J_{\mathbf{xy}} = \pm 1$, with 50% probability. The couplings are chosen at the start of the simulation and remain fixed (quenched disorder). A particular choice of couplings is termed a sample. In the absence of an external magnetic field ($H = 0$), this model undergoes a spin-glass transition at critical temperature $T_g = 1.102(3)$ (ref. 42).

The off-equilibrium dynamics was simulated with the Metropolis algorithm. The numerical time unit is the lattice sweep, which roughly corresponds to 1 ps of physical time.

In this work, we have simulated $N_S = 4$ samples using a lattice size of $L = 160a_0$. For each of these samples and for each protocol (Table 1), we have simulated $N_R = 512$ replicas (that is, independent simulations carried out for a given sample, following an identical protocol). We use replicas to account for thermal noise controlling the simulation (each replica is controlled by an independent realization of the thermal noise). The average over the thermal noise will be represented as $\langle\cdots\rangle$. Thereafter, we shall perform the average over samples, which will be indicated as $\overline{\langle\cdots\rangle}$.

However, on a few occasions (particularly for the analysis shown in the 'Measurement of Zeeman length through the scaling law of effective times' section), the final quantities are computed for a single sample (this is, of course, the approach followed in the laboratory). In these cases, the different samples allow us to assess to which extent our results depend on disorder realization (Supplementary Note I).

Besides, as a null experiment for temperature chaos, we have studied the link-diluted Ising model (DIM), also on cubic lattices of size $L = 160a_0$ with periodic boundary conditions and using Metropolis dynamics. Specifically, we used the Hamiltonian in equation (3) but with couplings $J_{\mathbf{xy}} = 1$ (with 70% probability) or $J_{\mathbf{xy}} = 0$ (with 30% probability) and magnetic field $H = 0$. Since all the couplings are positive or zero, this is a ferromagnetic system without frustration, for which no temperature chaos is expected. The critical temperature for the DIM is $T_c = 3.0609(5)$ (ref. 41) (actually, this is twice the value reported in another work[41] due to our use of an Ising formulation rather than a Potts formulation). In fact, with some abuse of language, in the main text, we refer to DIM temperatures as $T = 0.9$, $T = 0.7$ or 0.5 rather than to their actual values of $T = 0.9T_c/T_g$, $T = 0.7T_c/T_g$ or $0.5T_c/T_g$, respectively, where T_g is the critical temperature for the Edwards–Anderson model. We follow the very same procedure, which is explained in the 'Computation of ξ_{micro}' section, to compute the coherence length ξ_{micro} for both spin glass and DIM. We have chosen times for the DIM such that ξ_{micro} coincides with the corresponding spin-glass value, namely, $\xi_{\text{micro}} = 5.84$ (protocol A'_5 in Table 2), $\xi_{\text{micro}} = 10.11$ (protocol A'_7) and $\xi_{\text{micro}} = 16.63$ (protocol A'_9). Of course, the necessary times are extremely short for DIM than spin glass. Given that the DIM simulations were comparatively inexpensive, we simulated 16 samples (each with 512 replicas) for this model.

Some ZFC observables

As explained in the main text, our simulations are designed to mimic the experimental protocol called ZFC. In ZFC protocols, a sample initially in equilibrium at some very high temperature is cooled below T_g, always maintained at zero magnetic field. In the native protocols, the system is abruptly taken to the measuring temperature, where it is let to relax for time t_w. The cooling process (always without a field) is more complex for our jump protocols (Fig. 1).

For both protocols, native or jump, we let the system relax for time t_w at the final, measuring temperature. Then, the external magnetic field H is switched on and we record the magnetic density as

$$M_{\text{ZFC}}(t, t_w; H) = \frac{1}{N}\sum_{\mathbf{x}} \langle s_{\mathbf{x}}(t + t_w; H)\rangle, \tag{4}$$

which grows with t from its initial value $M = 0$ at $t = 0$. We also record the two-time autocorrelation function as

$$C_{\text{ZFC}}(t, t_w; H) = \frac{1}{N}\sum_{\mathbf{x}} \langle s_{\mathbf{x}}(t_w; 0) s_x(t + t_w; H)\rangle. \tag{5}$$

Note that C_{ZFC} is a monotonically decreasing function of time and $C_{\text{ZFC}} = 1$ at $t = 0$.

Measurement of Zeeman length through the scaling law of effective times

The method introduced in another work[25] to experimentally measure the spin-glass coherence length has recently been refined. Indeed, the scaling law introduced in other work[9,10] is a milestone for describing the magnetic response of a spin glass in both 'lab experiments' and 'numerical experiments'. We shall name ξ_{Zeeman} as the length scale extracted using these methods.

In experiments on a single-crystal CuMn sample, the main quantity evaluated is the relaxation function $S_{\text{ZFC}}(t, t_w; H)$, which exhibits a local maximum at time $t^{\text{eff}}{}_H \approx t_w$. Hence, one focuses on the H dependence of $t^{\text{eff}}{}_H$. On the numerical side, we carry out massive numerical experiments spanning from picoseconds to tenths of a second on the Janus II supercomputer, from which we can also extract $t^{\text{eff}}{}_H$. The numerical method proceeds as follows (other studies[9,10] provide a full discussion). One first changes the variable by considering S_{ZFC} as a function of $C(t, t_w; H)$ (equation (5)) rather than time. The peak is found at $C_{\text{peak}}(t_w)$. Finally, $t^{\text{eff}}{}_H$ is found by solving the equation $C(t^{\text{eff}}{}_H, t_w; H) = C_{\text{peak}}(t_w)$. A crucial advantage is that this equation can also be directly solved at $H = 0$.

The numerical $S_{\text{ZFC}}(t, t_w; H)$, however, shows two peaks: a t_w-independent peak at very short times and a second, physically interesting peak at $t \approx t_w$. Unfortunately, in fixed-temperature simulations (that is, native protocols) with very short t_w, the two peaks cannot be resolved (Fig. 1, bottom left). We have not attempted to extract ξ_{Zeeman} in native runs where the two peaks cannot be resolved. However, for the shortest jump protocol with $T_2 = 0.5$, namely, $t_w = 2^{10}$ and $2^{15.625}$, we could borrow C_{peak} from the jump with the largest t_w (unfortunately, the same trick did not work for native runs, because important consistency checks[29] were not passed in this case).

From a phenomenological point of view, the effective time $t^{\text{eff}}{}_H$ can be associated with the height of the largest free-energy barrier $\Delta_{\max}$ through the usual Arrhenius law[25]

$$\Delta_{\max} = k_B T(\log t^{\text{eff}}{}_H - \log \tau_0), \tag{6}$$

where k_B is the Boltzmann constant, τ_0 is the characteristic exchange time, $\tau_0 \approx \hbar/k_B T_g$, and h is the Planck constant. In an external magnetic

field, the free-energy barriers are lowered by the Zeeman energy E_Z (ref. 25). For a small magnetic field, E_Z behaves as

$$E_Z = \xi_{\text{Zeeman}}^{D-\theta/2}\chi_{\text{FC}}H^2, \tag{7}$$

which defines ξ_{Zeeman}. Here χ_{FC} is the field-cooled magnetic susceptibility per spin, $\xi_{\text{Zeeman}}^{D-\theta/2}$ is the number of correlated spins, $D = 3$ is the spatial dimension and θ is the replicon exponent[28].

We slightly depart from the previous approach by exploiting a scaling theory. We use the effective time $t^{\text{eff}}{}_H$ to reflect the total free-energy change at magnetic fields H and $H = 0^+$ (refs. 9,10):

$$\log\left[\frac{t_H^{\text{eff}}}{t_{H\to 0^+}^{\text{eff}}}\right] = \frac{\hat{S}}{2T}\xi_{\text{micro}}^{D-\theta/2}H^2 + \xi_{\text{micro}}^{-\theta/2}\mathcal{G}\left(T, \xi_{\text{micro}}^{D-\theta/2}H^2\right), \tag{8}$$

where $\hat{S}$ is a constant coming from the fluctuation–dissipation relations and $\mathcal{G}(x)$ is a scaling function behaving as $\mathcal{G}(x) \approx x^2$ for small $x = \xi_{\text{micro}}^{D-\theta/2}H^2$. For small-enough magnetic fields ($H \leq 0.017$), we can neglect the $\mathcal{O}(H^4)$ terms in equation (8):

$$\log\left[\frac{t_H^{\text{eff}}}{t_{H\to 0^+}^{\text{eff}}}\right] = c_2(t_w; T)H^2, \tag{9}$$

where we have included all the constants in the $c_2(t_w; T)$ coefficient.

Thus, fitting our data according to equation (9), we can define the Zeeman coherence length ξ_{Zeeman} as

$$\xi_{\text{Zeeman}}^{\text{jump}}(t_w, T_1 \to T_m) = \left[\frac{c_2(t_w, T_1 \to T_m)}{c_2(t_w{}^*, T_m)}\right]^{1/(D-\theta/2)} \xi_{\text{micro}}(t_w{}^*; T_m), \tag{10}$$

$$\xi_{\text{Zeeman}}^{\text{native}}(t_w, T_m) = \left[\frac{c_2(t_w, T_m)}{c_2(t_w{}^*, T_m)}\right]^{1/(D-\theta/2)} \xi_{\text{micro}}(t_w{}^*; T_m), \tag{11}$$

where $\xi_{\text{micro}}(t_w{}^*; T_m)$ plays the role of a reference length (the reference length allows us to avoid the precise determination of constants in equation (9)). The reference time $t_w{}^*$ is the longest available waiting time for our native runs at measuring temperature T_m. For the sake of clarity, in equations (10) and (11), we omit the explicit dependence of θ on ξ_{micro} (ref. 7).

Numerical coherence lengths ξ_{micro} and ζ

In this paragraph, we shall consider two more length scales. One of them, ξ_{micro}, is computed from the correlation function for the spin-glass order parameter (hence, ξ_{micro} tells us about the size of the glassy domains). The second length scale, $\zeta(t_1, t_2)$, tells us about how the system reorganizes itself when going from earlier time t_1 to later time t_2.

Computation of ξ_{micro}. For the reader's convenience, let us recall the definition of the spatial autocorrelation function that we use for computing $\xi_{\text{micro}}(t_w)$ (ref. 38):

$$C_4(\mathbf{r}, t'; T) = \overline{\langle q^{(a,b)}(\mathbf{x}, t')q^{(a,b)}(\mathbf{x}+\mathbf{r}, t')\rangle_T}, \tag{12}$$

$$q^{(a,b)}(\mathbf{x}, t') \equiv \sigma^{(a)}(\mathbf{x}, t')\sigma^{(b)}(\mathbf{x}, t'), \tag{13}$$

where $t' = t_w + t$, the indices (a, b) label different real replicas, and $\langle\cdots\rangle_T$ stands for the average over thermal noise at temperature T.

The calculation of the correlation function is computationally costly since we have $N_R(N_R-1)/2$ possible choices of the pair of replicas. Fortunately, it can be accelerated using the specific multispin coding methods explained elsewhere[43].

Once we have $C_4(\mathbf{r}, t'; T)$, we compute the integrals as[26,27,38]

$$I_k(t'; T) = \int_0^\infty \mathrm{d}^3 r\, r^k C_4\,(\mathbf{r} = (r, 0, 0), t'; T)\,. \tag{14}$$

A coherence length can be computed as

$$\xi_{k,k+1}(t', T) = \frac{I_{k+1}(t', T)}{I_k(t', T)}. \tag{15}$$

We define $\xi_{\text{micro}}(t, t_w; H) = \xi_{12}(t, t_w; H)$.

The ζ length scale. This length scale was studied in detail in another work[38] by refining earlier suggestions[39,40].

Let us consider the thermal trajectory followed by a given replica at two times t_1 and t_2 ($t_1 < t_2$). Our basic quantity will be the local correlation

$$c_{\mathbf{x}}(t_1, t_2) = s_{\mathbf{x}}(t_2)s_{\mathbf{x}}(t_1). \tag{16}$$

Note that $c_{\mathbf{x}}(t_1, t_2) = -1$ if the spin at site $\mathbf{x}$ has been flipped when going from time t_1 to time t_2 (otherwise, $c_{\mathbf{x}}(t_1, t_2) = 1$). Then, the two-time, two-site correlation function is

$$C_{2+2}(\mathbf{r}, t_1, t_2) = \frac{1}{N}\sum_{\mathbf{x}} \overline{[\langle c_{\mathbf{x}}(t_1, t_2)c_{\mathbf{x}+\mathbf{r}}(t_1, t_2)\rangle - C^2(t_1, t_2)]}, \tag{17}$$

where

$$C(t_1, t_2) = \frac{1}{N}\sum_{\mathbf{x}} \langle c_{\mathbf{x}}(t_1, t_2)\rangle. \tag{18}$$

The ideal $\zeta(t_1, t_2)$ is defined from the long-distance decay of $C_{2+2}(\mathbf{r}, t, t_w)$:

$$C_{2+2}(\mathbf{r}, t_1, t_2) \approx \frac{1}{r^b}\, g(r/\zeta(t_1, t_2)), \tag{19}$$

where g is an unknown scaling function. We bypass our lack of knowledge of g exactly as we solved this problem for ξ_{micro}: by using integral estimators (equation (15)). Note that by construction, $\zeta(t_1, t_2)$ tends to zero when t_2 approaches t_1. Conversely, we expect $\zeta(t_1, t_2)$ to grow with later time t_2.

As for the interpretation of length scale ζ, an analogy with the theory of liquids can help. We name a defect a site where $c_{\mathbf{x}}(t_1, t_2) = -1$. Let $n(t_1, t_2)$ be the density of defects ($C(t_1, t_2) = 1 - 2n(t_1, t_2)$) and let $g(\mathbf{r})$ be the pair-correlation function for defects: the conditional probability for having a defect at site $\mathbf{x} + \mathbf{r}$, given that a defect is present at site $\mathbf{x}$, is $n(t_1, t_2)g(\mathbf{r})$ (such that at long distances, $g(\mathbf{r})$ tends to one). Given these definitions, one easily finds that

$$C_{2+2}(\mathbf{r}, t_1, t_2) = 4\,\overline{n^2(t_1, t_2)\,[g(\mathbf{r}) - 1]}. \tag{20}$$

In other words, ζ is the length scale on which the defects are correlated. Only when $\zeta(t_2, t_1) \approx \xi_{\text{micro}}(t_1)$, the configuration at time t_2 starts to structurally differ from the configuration at earlier time t_1.

Finally, let us mention that a length analogous to $\zeta(t_1, t_2)$ can be obtained with the analysis tools of temperature chaos (Supplementary Note IV).

Computation of the chaotic parameter

As explained in the main text, our goal here is to introduce a correlation parameter that will allow us to compare two different thermal protocols. This comparison should necessarily be local in space. To this end, we adapt the procedure introduced elsewhere[37].

Specifically, we select $N_{\text{sph}} = 8{,}000$ spheres of radius R randomly chosen inside the system and centred at the central points of the elementary cells of the cubic lattice. Now, let us consider two identical systems that are subjected to two different thermal protocols, named

protocols A_1 and A_2. Next, we perform a set of independent simulations (that is, replicas) for protocol A_1, and another set of independent simulations for protocol A_2. Then, the correlation coefficient for protocols A_1 and A_2 as computed on the kth sphere of radius R is defined as

$$X^{k,R}_{A_1,A_2} = \frac{\left\langle \left[q^{k,R}_{A_1,A_2}\right]^2 \right\rangle_T}{\sqrt{\left\langle \left[q^{k,R}_{A_1,A_1}\right]^2 \right\rangle_T \left\langle \left[q^{k,R}_{A_2,A_2}\right]^2 \right\rangle_T}}. \quad (21)$$

In the above expression, $q^{k,R}_{A_1,A_2}$ is the overlap between two replicas σ and τ that have undergone thermal protocols A_1 and A_2, respectively,

$$q^{k,R}_{A_1,A_2} = \frac{1}{N_r} \sum_{\mathbf{x}\in B^k_R} s^{\sigma,A_1}_{\mathbf{x}} s^{\tau,A_2}_{\mathbf{x}}, \quad (22)$$

where N_R is the number of spins within the kth sphere B^k_R of radius R.

The interpretation of the chaotic parameter is very similar to a correlation coefficient: if $X^{k,R}_{A_1,A_2} = 1$, spin configurations from thermal protocols A_1 and A_2 are completely indistinguishable inside the sphere B^k_R (absence of chaos). Instead, $X^{k,R}_{A_1,A_2} = 0$ corresponds to completely different configurations, which is an extremely chaotic situation.

The reader may notice from equation (21) that the computation of $X^{k,R}_{A_1,A_2}$ involves an exact thermal expectation value (which could be obtained in simulations only if one had simulated an infinite number of replicas). Unfortunately, we only have $N^{\max}_R = 512$ replicas at our disposal. Our choice has been to produce different estimates of $X^{k,R}_{A_1,A_2,N_R}$ by varying N_R. Specifically, our procedure has been the following:

1. For each $N_R < N^{\max}_R$, we randomly order the $N^{\max}_R$ replicas and divide them in $N^{\max}_R/N_R$ groups of N_R replicas.
2. In this way, we get $N^{\max}_R/N_R$ independent estimates of $X^{k,R}_{A_1,A_2,N_R}$.
3. To erase the effect of the initial permutation of the $N^{\max}_R$ replicas, we repeat this procedure ten times for all $N_R < N^{\max}_R$.

In a nutshell, for every sphere of radius R, we obtain $N_{\text{thermal}}(N_R)$ estimates of $X^{k,r}_{A_1,A_2,N_R}$, where

$$N_{\text{thermal}}\left(N_R < N^{\max}_R\right) = 10 \times \frac{N^{\max}_R}{N_R}, \quad (23)$$

or

$$N_{\text{thermal}}\left(N_R = N^{\max}_R\right) = 1. \quad (24)$$

We average the N_{thermal} estimates of $X^{k,R}_{A_1,A_2,N_R}$ for every N_R and finally, in a complete analogy with ref. 37, we compute the extrapolation of the chaotic parameter to an infinite number of replicas by means of a simple linear extrapolation:

$$X^{k,R}_{A_1,A_2,N_R} = X^{k,R}_{A_1,A_2,\infty} + \frac{A^{k,R}_{A_1,A_2}}{N_R}, \quad (25)$$

where $X^{k,R}_{A_1,A_2,\infty}$ is our best estimation of $X^{k,R}_{A_1,A_2}$. More complicated extrapolations do not seem to present advantages[37].

Finally, to explore the statistical information carried by the $N_{\text{sph}} = 8{,}000$ spheres, we define the distribution function as

$$F(\tilde{X}, A_1, A_2, R) = \text{Probability}\left[X^{k,R}_{A_1,A_2} < \tilde{X}\right]. \quad (26)$$

Some examples of this distribution function are displayed in Fig. 4.

Data availability

The data contained in the figures of this paper, accompanied by the gnuplot script files that generate these figures, are publicly available via GitHub at https://github.com/janusII/Rejuvenation_memory.git. The data that support the findings of this study are available from the corresponding author upon reasonable request.

Code availability

The codes that support the findings of this study are available from the corresponding author upon reasonable request

References

43. Paga, I. *From Glassy Bulk Systems to Spin-Glass Films: Simulations Meet Experiments*. PhD thesis (Complutense Univ. of Madrid and University of Rome, La Sapienza, 2021).

Acknowledgements

We acknowledge the valuable contributions and ideas of our collaborator Raffaele Tripiccione. The Janus project would have been impossible without his technical expertise. We thank R. Orbach for discussions. This work was partly supported by grants nos. PID2020-112936GB-I00, PID2019-103939RB-I00, PGC2018-094684-B-C21, PGC2018-094684-B-C22 and PID2021-125506NA-I00 funded by MCIN/AEI/10.13039/501100011033 by "ERDF A way of making Europe" and by the "European Union; and by the Atracción de Talento program (ref. 2019-T1/TIC-12776) funded by Comunidad de Madrid and Universidad Complutense de Madrid (Spain). This project has received funding from the European Research Council under the European Union's Horizon 2020 research and innovation programme (grant no. 694925; G.P.). We were also partly supported by ICSC – Centro Nazionale di Ricerca in High Performance Computing, Big Data and Quantum Computing, funded by the European Union – NextGenerationEU. I.G.-A.P. was supported by MCIU (Spain) through FPU grant no. FPU18/02665. J.M.-G. was supported by the Ministerio de Universidades and the European Union 'NextGenerationEU/PRTR' through a 2021–2023 Margarita Salas grant. We thank the Spanish Supercomputing Network (RES) for providing access to its Data Storage program at its BIFI (University of Zaragoza) node. IP was supported by LazioInnova-Regione Lazio under the program Gruppi di ricerca2020 - POR FESR Lazio 2014-2020, Project NanoProbe (Application code A0375-2020-36761). BS was partially supported by the Banco Santander and the Complutense University of Madrid through the grant PR44/21-29937.

Author contributions

D.I. and A.T. contributed to the design of the Janus II project. J.M.G.-N. and D.N. contributed to the Janus II/Janus simulation software. M.B.-J., E.C., A.C., L.A.F, J.M.G.-N., I.G.-A.P., A.G.-G., D.I., A.M., A.M.S., I.P., S.P.-G., S.F.S. and A.T. contributed to the Janus II hardware and software development. L.A.F., E.M., V.M.-M. and I.P. suggested undertaking this project. L.A.F., E.M., V.M.-M., I.-P., F.R.-T. and J.J.R.-L. designed the research. J.M.-G. and I.P. analysed the data. M.B.-J., L.A.F., E.M., V.M.-M., J.M.-G., I.P., G.P., B.S., J.J.R.-L., F.R.-T. and D.Y. discussed the results. L.A.F., E.M., V.M.-M., J.M.-G., I.P., J.J.R-L., B.S., F.R.-T. and D.Y. wrote the paper.

Competing interests

The authors declare no competing interests.

Additional information

Supplementary information The online version contains supplementary material available at https://doi.org/10.1038/s41567-023-02014-6.

Correspondence and requests for materials should be addressed to I. Paga.

Peer review information *Nature Physics* thanks Eric Vincent, Peter Young and the other, anonymous, reviewer(s) for their contribution to the peer review of this work.